Nanomed. J. 6(1):55-66, Winter 2019

RESEARCH PAPER

BSA nanoparticles loaded with IONPs for biomedical applications: fabrication optimization, physicochemical characterization and biocompatibility evaluation

Parvin Najafi Anamaghi, Hasan Kouchakzadeh *

Protein Research Centre, Shahid Beheshti University, G. C. Velenjak, Tehran, Iran

ABSTRACT

Objective(s): Cancer diagnosis in its early stages of progress, can enhance the efficiency of treatment utilizing conventional therapy methods. Non-biocompatibility of iron oxide nanoparticles (IONPs) has made a big challenge against their usage as a contrast agent. Efficient coverage by biomolecules such as albumin can be a solution to overcome this problem. Herein, albumin-coated IONPs were prepared and the process was optimized using the response surface methodology (RSM) to achieve optimum loading of IONPs in albumin nanoparticles.

Materials and Methods: IONPs were incorporated into bovine serum albumin nanoparticles (BSA NPs) matrix, to yield IONPs-BSA NPs. The resulting nanoparticles were characterized physicochemically by scanning electron microscopy (SEM), dynamic light scattering (DLS), inductively coupled plasma optical emission spectrometry (ICP-OES), Fourier transform infrared spectroscopy (FTIR) and vibrating sample magnetometer (VSM). The stability test was conducted over 6 months.

Results: Under optimum conditions of 2.28 mg for iron weight and pH 9.21, loading of 7.76% was obtained for the spherical IONPs-BSA NPs with the size of 177±12 nm, PDI of 0.222±0.07 and zeta-potential of -36.4±2.3 mV. These findings revealed that more than 90% and 60% of the particles retained their size over four and six months of storage at 4 ˚C, respectively. In addition, non-cytotoxicity and hemocompatibility of IONPs-BSA NPs were verified in vitro thereby offering them as a biocompatible contrast agent for cancer diagnosis.

Conclusion: The IONPs-BSA NPs developed in this study are promising to be further investigated and functionalized with a ligand to obtain a targetable MRI contrast agent for early cancer diagnosis.

Keywords: *Bovine serum albumin nanoparticles, Iron oxide nanoparticles, Optimum production; Response surface methodology (RSM)*

How to cite this article

Najafi Anamaghi P, Kouchakzadeh H. BSA nanoparticles loaded with IONPs for biomedical applications: fabrication optimization, physicochemical characterization and biocompatibility evaluation. Nanomed J. 2019; 6(1): 55-66. DOI: 10.22038/nmj.2019.06.008

INTRODUCTION

Cancer diagnosis in its early stages of progress can increase the chance of successful treatment. Improved contrast agents for medical imaging procedure play a pivotal role for the early diagnosis of cancer [1, 2]. Magnetic resonance imaging (MRI), as one of the powerful techniques in cancer diagnosis, offers the advantages of non-invasive, multiparametric imaging, deep soft tissue penetration, non-ionizing, being harmless to patients, giving high-resolution images with an excellent soft tissue contrast between different tissues [3–5]. Development of MRI contrast agents with high efficiency and sensitivity is essential for achieving a successful bio-imaging at the cellular and molecular level [4, 6–9]. Among the magnetic-based contrast agents that can be employed for MRI imaging, super paramagnetic iron oxide NPs (SPIONs) like Fe_3O_4 and Fe_2O_3 are widely used due to their chemical stability, biodegradability and low toxicity. IONPs are sensitive and negative MRI probes possessing the ability to noninvasively monitor events occurring on the cellular and even molecular levels *in vivo* [10–15].

Biological applications of IONPs are limited because of their high surface hydrophobicity that make them prone to being engulfed by macrophages and rapid clearance from blood circulation. To prolong the circulation half-life of the IONPs, it is essential to modify their surface for increasing their hydrophilicity. Both organic

* *Corresponding Author Email: h_kouchakzadeh@sbu.ac.ir*

Note. This manuscript was submitted on November 2, 2018; approved on December 1, 2018

polymers and inorganic materials can be used for the encapsulation of IONPs. One of the main approaches is the entrapment of IONPs into the matrix of NP, such as albumin NPs or polymers such as polycaprolactone (PCL), poly lactic acid (PLA), poly lactic-co-glycolic acid (PLGA), dextran and chitosan [16, 17].

Albumin is the major soluble protein in blood plasma (35-50 g/l). It is well-known for its versatile nature with an important role in the transportation and distribution of several compounds, such as drugs, hormones, amino acids, and fatty acids [18]. Albumin-based nanocarriers have been considered for clinical applications due to their advantages such as availability, excellent biodegradability, preferential uptake in tumors and inflamed tissues [19]. Abraxane® (paclitaxel-human serum albumin NPs)-a commercial available product-is approved by US FDA for the treatment of metastatic breast cancer. Clinical studies of Abraxane® verified that human serum albumin (HSA) based NPs have no adverse effects *in vivo* [20, 18].

Albumin is not captured by macrophages in the liver [21]. Thus, phagocytosis by the reticuloendothelial system (RES) can be inhibited by loading of IONPs into albumin NPs resulting in the prolongation of serum half-life of IONPs enabling the enhanced permeability and retention (EPR) effect *in vivo*. Owing to the EPR effect, intravenously administered albumin modified IONPs can be extravasated from the vasculature, and preferentially accumulated in tumor tissue. This passive targeting mechanism has the advantages of reducing IONPs uptake in liver and spleen and achieving high concentrations of IONPs in tumor [9].

Designing of albumin complexes has paved the way for carriers with prolonged blood circulation times. The most commonly adopted approach to form albumin corona on NPs involves incubation of NPs with albumin which results in physical adsorption of the protein on the NP surface. Separation of the albumin–NP complex achieve by centrifugation followed by washing to remove the unbounded proteins. Coating these nanohybrids with specific ligands can enable targeting of tumor cells and specific organs. Stability of albumin over a wide range of pH, is one of the characteristics of albumin–NP conjugates that give them an edge over other nanocarriers [22, 23].

Herein, hydrophobic IONPs as a potential contrast agent were loaded physically into bovine serum albumin (BSA) NPs, which is different from the conjugation or coating approach. An optimized desolvation method was developed for optimum loading of IONPs into BSA NPs. Main effective and independent factors were identified, and loading process was optimized using response surface methodology (RSM)-central composite design (CCD) of the experiments by design expert software (DX-7, State-Ease Inc, version 7.0.0). After analyzing the results and obtaining the optimum conditions, the IONPs-BSA NPs were characterized physicochemically by scanning electron microscopy (SEM), dynamic light scattering (DLS), inductively coupled plasma optical emission spectrometry (ICP-OES), Fourier transform infrared spectroscopy (FTIR) and vibrating sample magnetometer (VSM). Then, NPs prepared under the optimum conditions, were evaluated for the cellular toxicity and hemocompatibility *in vitro*. In addition, the long-term physicochemical stability of optimized IONPs-BSA NPs iwas nvestigated during six months of storage to determine the storage conditions of this novel nano biomedicine system.

MATERIAL AND METHODS

Chemical and biological materials

Bovine serum albumin (BSA, purity 96–99%), glutaraldehyde 8% aqueous solution, 3-(4,5-dimethyl thia-zol-2-yl)-2,5-diphenyl tetrazolium bromide (MTT) and dimethyl sulfoxide (DMSO) were purchased from Sigma-Aldrich. Ferric chloride hexahydrate ($FeCl_3.6H_2O$), ferrous chloride tetrahydrate ($FeCl_2.4H_2O$), ethanol, hydrochloric acid (HCl), ammonia and all other reagents were of analytical grades and used as received.

Breast cancer cell line, MCF-7, was obtained from National Cell Bank of Iran (NCBI, Pasteur Institute of Iran, Tehran, Iran) and cultured in RPMI 1640 culture medium (Gibco, Invitrogen, Carlsbad, CA) containing 15% fetal bovine serum (FBS) (Gibco Invitrogen), 100 µg/ml streptomycin, and 100 U/ml penicillin (Gibco Invitrogen), and incubated at 37 °C in humidified atmosphere containing 5% CO_2.

Synthesis of IONPs

The IONPs were produced by a Massart coprecipitation method [2, 5, 23], based on the reaction between iron (II) and iron (III) ions in an aqueous ammonia solution to form magnetite, Fe_3O_4, as shown in equation (1):

$$2FeCl_3+FeCl_2+8NH_3+4H_2O \rightarrow Fe_3O_4+8NH_4Cl$$

Briefly, 1.0 ml of stock $FeCl_2$ solution and 4.0 ml

of stock $FeCl_3$ solution mixed together and stirred vigorously by a magnetic stirring device. Then, 50 ml of 2 M aqueous NH_3 solution was added slowly into the flask, leading to the formation of a black colloidal suspension of magnetite iron oxide NPs. Finally, the suspension was centrifuged (Shanghai Zhizhege Co, Ltd) for 30 min at 20,000 rpm in order to separate the magnetic particles. The supernatant was collected and stored after centrifugation.

Production of IONPS-BSA NPs

The IONPs-containing BSA NPs (IONPs-BSA NPs) were prepared by a desolvation technique as mentioned previously [24, 25]. Desolvation is the most commonly used method as it leads to the production of albumin NPs with size of less than 200 nm [20]. In brief, different weights of iron in terms of IONPs, from 1 mg to 2.5 mg were added to 2 ml of BSA aqueous solution (200 mg BSA in 2 ml distilled water) which was adjusted to desired pH using 1 N NaOH. Afterwards, ethanol was added continuously at a constant rate (1 ml/min) into the IONPs-BSA aqueous solution and finally, 100 µl of glutaraldehyde 8% was added dropwise under constant stirring (550 rpm) [26, 27]. The suspension then was stirred for another eight hours at room temperature in order to complete the crosslinking reaction [28]. The particles were purified by three cycles of centrifugation (10 min × 10,000 rpm, Spetrafuge, Labnet International Inc, EDISON, NJ, USA), continued with resuspension of the centrifugation pellet in distilled water to the original volume to remove excess glutaraldehyde, unreacted chemicals, free BSA molecules and unloaded IONPs using an ultrasonic water bath (EURONDA 4D, Italy 50/60 Hz, SN: EGC1 10081). The amount of IONPs-BSA NPs and unloaded IONPs were determined gravimetrically and inductively coupled plasma optical emission spectrometry (ICP-OES) methods, respectively.

Determination of the effective experimental factors and their levels

It was found that a wide variety of factors such as ethanol concentration, the cross-linking reaction temperature, ethanol addition rate, glutaraldehyde concentration, pH, the cross-linking reaction time, stirring rate, type of desolvating agent (ethanol, methanol or acetone) and iron weight, could influence the preparation process [24, 29, 30].

The effect of some of these factors such as ethanol addition rate, glutaraldehyde concentration, stirring rate and desolvating agent type was determined according to the literatures [16, 24, 26]. Two factors consisting of iron weight and pH remained undefined and considered as the main factors affecting the preparation process. These two factors need cooperative optimization to obtain NPs with efficient IONPs loading. pH (A) and iron weight in terms of IONPs (B) considered as the most important independent factors affecting the loading efficiency and their levels were determined after some preliminary experiments. The lowest and highest levels of iron weight in 100 mg/ml BSA solution determined as 1 to 2.5 mg, respectively.

The pH range of 7.5 to 9.5 was selected as the lowest and highest levels, respectively. In addition, the IONPs-BSA incubation time was evaluated and adjusted to be eight hours after glutaraldehyde addition. The factors and their levels are shown in Table 1.

Design of experiments by response surface methodology

In order to investigate the optimization of IONPs loading in BSA nanoparticles, experiments were designed using RSM-central composite design (CCD) of experiments by DX-7 software [29, 31]. Afterward, thirteen experiments conducted (Table 2); four of them were organized in a full factorial design and four experiments were related to axial points. The other five experiments involved repetition of the central design to obtain a good estimate of the experimental error.

Optimization of IONPs loading

The iron content of the magnetic nanosystem

Table 1. Selected factors and their levels used for experimental design.

Variables		Coded Value				
Name	Unit	−α	−1	0	+1	+α
A	pH	7.5	7.79	8.5	9.21	9.5
B	Weight of iron in terms of IONPs (mg)	1	1.22	1.75	2.28	2.5

Table 2. Design of experiments by RSM-CCD using DX-7 for the optimization of IONPs loading

Run	Factor 1	Factor 2
	A: pH	B: IONPs (mg)
1	9.21	2.28
2	8.50	2.50
3	7.50	1.75
4	8.50	1.75
5	8.50	1.75
6	8.50	1.00
7	8.50	1.75
8	7.79	1.22
9	9.50	1.75
10	7.79	2.28
11	9.21	1.22
12	8.5	1.75
13	8.50	1.75

was determined by ICP spectroscopy (ICO-OES, Arcos, Spectro, Germany) at 238.204 nm wavelength after each experiments. For this purpose, the iron content in the supernatants after the purification step was quantified by ICP-OES and the amount of IONPs loading was calculated using a standard curve and the initial amount of iron according to Eq (2).

Loading(%)=(weight of IONPs in NPs)/(weight of NPs)×100

Physicochemical characterization of the nanoparticles

IONPs-BSA NPs prepared under optimum conditions were characterized with respect to their average particle size, size distribution (PDI), and zeta potential by DLS (Malvern Instrument, Serial Number: MAL1001767). For this purpose, the samples were diluted with distilled water before the measurements (n=3). All measurements performed at room temperature and scattering angle set to 90°. The results are reported as mean±standard deviation (S.D.). FTIR was used to determine the formation of the IONPs-BSA NPs. The binding state of the IONPs with BSA NPs was evaluated using a FTIR spectrometer (PerkinElmer-Frontier) at room temperature in the frequency range of 4,000-500 cm^{-1}. In this regard, samples of IONPs, BSA NPs and IONPs-BSA NPs were freeze-dried, then mixed with KBr to obtain pellets for FTIR analyses. The magnetic properties of unmodified IONPs and optimized IONPs-BSA NPs studied on a VSM under an applied magnetic field. The hysteresis of the magnetization was obtained by changing external fields (H) between -8,000 and +8,000 G and operating at 300 k. For this purpose, both samples dried before the measurements. To verify the morphology of IONPs-BSA NPs, a scanning electron microscopy (KYKY-EM3200 model, China) method was employed. Sample dried on a glass slide and coated with gold using a sputter coater at an acceleration voltage of 2.0 kV. Then the sample assessed under a SEM using an acceleration voltage of 26.0 kV with the magnification of 40 k.

Long-time stability investigation of IONPs-BSA NPs

For the evaluation of the long-time storage stability of optimized IONPs-BSA NPs, physicochemical specifications consisting of particle size, PDI and zeta potential were measured 0, 2, 4 and 6 months after production by DLS. In this regards, the produced nanoparticles kept at 4 °C in refrigerator and analyzed according to time table schedule.

Hemolysis assay

In order to investigate the biocompatibility of albumin-coated magnetic NPs, hemolysis assay was performed on a fresh human blood stabilized with EDTA. Before the hemolysis assay, HRBCs were separated from the blood sample according to the procedure reported in the literature [6]. In brief, the blood was centrifuged (1,000 rpm, 5 min) to remove the supernatant and washed with phosphate buffer saline (PBS) for 5 times in order to completely remove serum and obtain the HRBCs. Thereafter, the HRBCs were diluted 10 times with PBS. The diluted HRBC suspension (0.1 ml) was transferred into 2-ml microtubes prefilled with 0.9 ml deionized water (as positive control), 0.9 ml PBS (as negative control), and 0.9 ml PBS containing either IONPs or IONPs-BSA NPs with different iron concentrations (50, 100, 200 and 400 µg/ml), respectively. The mixtures were kept at room temperature for two hours after a gentle shaking. After centrifugation (1,000 rpm, 5 min), the absorbance of the supernatants was recorded by a plate reader (Infinite 200 PRO-Life Sciences) and the hemolysis percentages of different samples was calculated by dividing the difference in absorbance at 541 nm between the

sample and the negative control by the difference in absorbance at 541 nm between the positive and negative controls (n=3).

In vitro cytotoxicity test

MTT assay was employed for the assessment of the cytotoxicity of the IONPs-BSA NPs *in vitro*. MCF-7 cells were seeded on 96-well plates (20,000 cells per well) and incubated with the IONPs-BSA, unmodified IONPs and BSA NPs dissolved in RPMI 1640 with FBS 10 %, at different iron concentrations (0, 25, 50, 75, and 100 µg/ml). After incubation for 24 and 48 h, 100 µl of MTT (5 mg/ml) was added to each well and the cells were incubated for another 4 h. Afterward, the medium was removed and DMSO (100 µl/well) was added to dissolve the formazan crystals. The absorbance of each well was monitored by a microplate reader at 600 nm. The relative cell viability (RCV) relative to the control wells was calculated by the following equation: RCV = $(OD_{test}/OD_{control}) \times 100\%$, where OD_{test} and $OD_{control}$ are obtained in the presence and absence of the magnetic NPs (n=3), respectively.

Statistical analysis

The relationships between responses and variables of all models were derived by DX-7. Statistical analyses including response surface analyses were conducted. In order to construct the final equations, significant terms with the consideration of *P*-values less than 0.05 were chosen. The suitability of quadratic models was confirmed by values of R^2 and one-way analyses of variance (ANOVA) at the probability level of 0.05.

RESULTS

The objective of the present study was the development of a biocompatible nanosystem that can be employed for diagnostic applications. The production process was optimized, IONPs loaded BSA nanoparticles were characterized physicochemically and evaluated *in vitro* in terms of cytotoxicity and hemocompatiblity.

Construction of model equations

IONPs were produced by a coprecipitation method. The obtained IONPs showed average size of 8 nm by DLS and PDI of 0.222. According to the literature, while iron weight and pH were considered as the most important independent input variables, IONPs loading in BSA NPs was the main dependent output variable for the optimization of loading process through the response surface methodology. In CCD-RSM, thirteen experiments were performed for two factors at five levels. The experimental results of CCD were fitted with a second order polynomial equation. The values of regression coefficients were calculated by DX-7 and the fitted equation for the prediction of loading was found to be:

Loading (%)= +5.25+1.43A+0.42B-0.23AB+0.17A2 +0.16B2

where all variables are in coded values and A is pH and B is the iron weight (mg) in terms of IONPs. The results of the analyses of variance (ANOVA) for the developed models, quadratic and interaction terms are listed in Table 3. Statistical significance of the model equations is evaluated by the Fisher variance ratio (F-value). F-value is a statistically valid measure of how well the factors describe the variation in the data around its mean. The greater F-value is from unity, the more certain it is that the factors adequately explain the variation in the data around its mean and that the estimated factor effects are real. The ANOVA of the regression models demonstrates that the models are highly significant, as evident from the Fisher's F-test (Fmodel for Loading = 37.73). The goodness of the fit with these quadratic models was confirmed by the determination coefficient (R^2). In this case, the values of the determination

Table 3. Analysis of variance (ANOVA) results obtained from design expert software for the main responses

Response	Loading (%)		
	Degree of freedom	F-value	P-value
Model	5	37.73	< 0.0001
A	1	168.55	< 0.0001
B	1	14.54	0.0066
AB	1	2.19	0.1824
A^2	1	2.04	0.1966
B^2	1	1.74	0.2281

A: pH
B: iron weight

coefficient ($R^2$for Loading = 0.9642) indicates that 96 percent of the variability in the response could be explained by the loading model. Fig 1 represents the comparison of the predicted and measured IONPs loading efficiency obtained from model simulation and experiments, respectively.

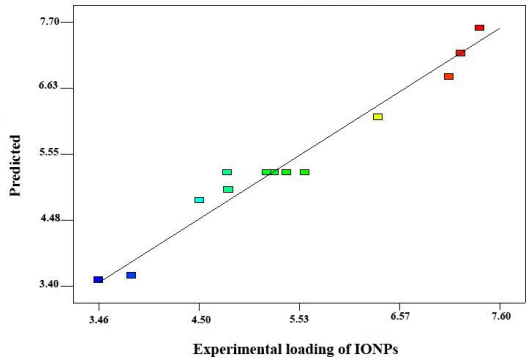

Fig 1. Predicted and actual IONPs loading efficiency (%) obtained from model simulation and experiments, respectively. Points are the actual amount of IONPs loading efficiency that approximately fit the model due to high amount of R2 (0.96)

The significance of each term is determined by P-value. The values of P<0.05 indicate the importance of the term. According to the ANOVA table and based on P-values, the first order main effects of iron weight and pH were significant. With the consideration of P-values, the first order main effects of parameters and main effects of variables on the main response are presented in Fig 2. According to the P-values (Table 3), interaction of variables has no significant effect on the loading efficiency. Fig 3, shows the effect of iron weight and pH on the loading. It is indicated that the loading value depends more on the pH rather than iron weight.

The loading efficiency clearly increased with increasing in pH. However, at high pH values, the loading efficiency increased with increasing in iron weight due to its more significance in comparison with iron weight.

These observations can be justified by considering Fig 2A, in which the pH has shown to have a positive effect on the loading efficiency. According to Fig 2A, the loading efficiency increases with increasing pH from 7.71 to 9.21 that is due to its positive first order and second order effects. Meanwhile, pH has been more significant factor affecting the loading efficiency in comparison with the iron weight according to the P-values.

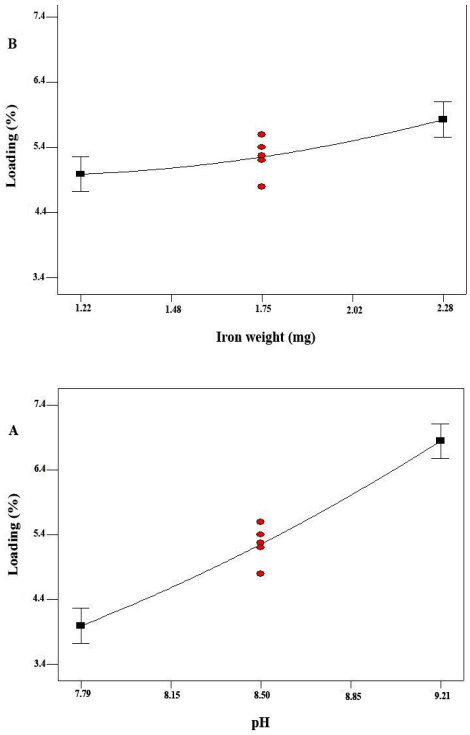

Fig 2. Main effects of pH (A) and iron weight (B) on IONPs loading (%) according to ANOVA table and obtained results. Main effects are significant on loading efficiency

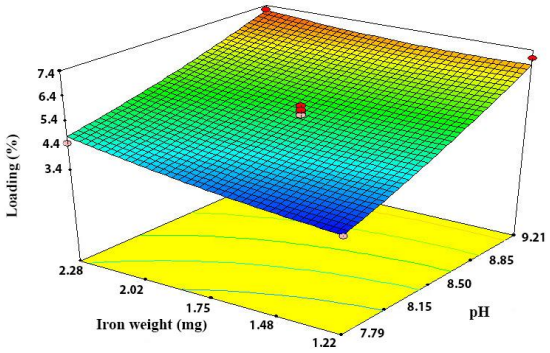

Fig 3. Effect of IONPs weight and pH on the IONPS loading efficiency. IONPs weight and pH have shown positive effects on the IONPs loading efficiency. pH has been the most significant factor affecting the IONPs loading efficiency in comparison with the IONPs weight

Determination of conditions for loading optimization

Design of Experiments (DOE) plays an important role in simultaneous investigation of the effects of various factors and thereby facilitating process optimization. In this study, an optimization technique was used by the DX-7 software based on the criterion of desirability for the optimization of loading efficiency as the main response. Table 4

Table 4. Predicted conditions by design expert software for optimum production of IONPs-BSA NPs

Response	Target	pH	Iron weight (mg)	Loading Prediction (%)
Loading (%)	Maximize	9.21	2.28	7.77

shows optimum conditions. The maximum loading (7.77%) was predicted at 2.28 mg iron and pH 9.2. To confirm the model accuracy reported by DX-7, additional experiments were performed under the predicted optimum condition in triplicate. These experiments yielded an average loading efficiency of 7.71±0.23 %. The good agreement between the predicted and experimental results confirmed the validity of the model and existence of the optimal point.

Therefore, these conditions considered as the optimum in order to achieve the maximum loading efficiency of IONPs in BSA NPs and used in the production process of IONPs-BSA NPs.

Physicochemical characterization of IONPs-BSA NPs

NPs produced under the optimum conditions were characterized by DLS (distilled water was used as the media for DLS analysis).

The average size, zeta potential and PDI of IONPs-BSA NPs obtained to be 177±12 nm, -36.4±2.3 mV and 0.222±0.07, respectively.

The results indicated that the IONPs-BSA NPs were negatively charged with proper particle size to be used as a diagnostic agent. Low PDI value demonstrated the narrow size distribution of the formulation. SEM micrograph of IONPs-BSA NPs verified their spherical shape with a narrow size distribution as shown in Fig 4.

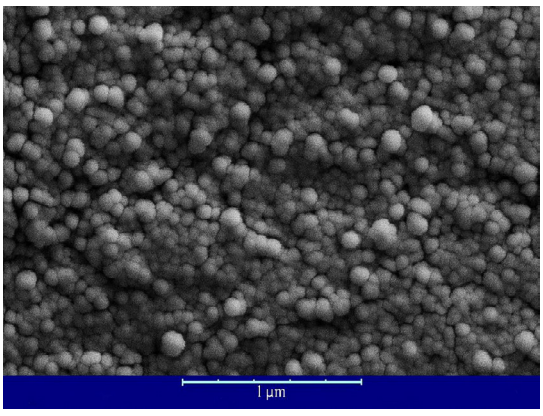

Fig 4. SEM micrographs of IONPs-BSA NPs prepared under optimum conditions, at magnification of 40,000×

Fig 5 shows the FTIR spectrum analysis. The absorption bands of BSA NPs were observed at 3303 cm^{-1} (amide A, related to N–H stretching), 2957 cm^{-1} (amide B, N–H stretching of NH^+ free ion), 1657 cm^{-1} (amide I, C=O stretching), 1534 cm^{-1} (amide II, related to C–N stretching and N–H bending vibrations), 1396 cm^{-1} (CH_2 bending groups) and ~1259 cm^{-1} (amide III, related to C–N stretching and N–H bending). The spectra of IONPs–BSA NPs exhibited these bands, however the absorption bands of N-H stretching of the amine groups was shifted from 3303 cm^{-1} to 3297 cm^{-1} and from 1259 cm^{-1} to 1254 cm^{-1} when BSA NPs were compared with IONPs-BSA NP. The FTIR spectrum of the IONPs shows the peak at 599 cm^{-1} corresponding to Fe-O in IONPs. The related changes in the amide A and III bands confirm the formation of IONPs-BSA NP. In addition, some bands showed different intensity, such as a decreased intensity in the amide I (5% decrease) and amide II (5% decrease) bands, indicating changes in the C–N and/or NH bonds, due to interactions of different groups on BSA.

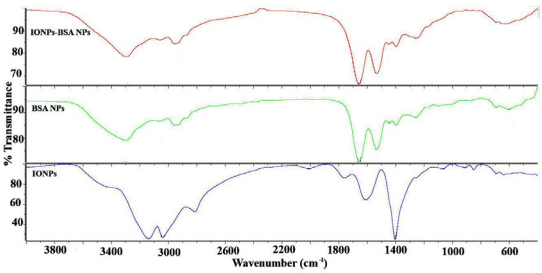

Fig 5. FTIR spectra of the IONPs (IONPs; blue), BSA NPs (BSA NPs; green) and IONPs-BSA NPS (IONPs-BSA NPS; red)

For VSM analysis, IONPs and IONPs-BSA NPs were dried prior to the evaluation of their magnetic properties.

The magnetic hysteresis loop characterizes the responses (magnetization) of magnetic materials to an external magnetic field. Results showed that IONPs and IONPs-BSA NPs do not retain any magnetism after removal of the magnetic field. In other words, they showed an absence of hysteresis and zero remanence after removal of the magnetic field [12]. Fig 6 shows plot of magnetization versus applied magnetic field. Both synthesized IONPs and IONPs-BSA NPs show superparamagnetic behavior, as evidenced by the zero remanence on the magnetization loops.

The saturation magnetization (M_s) of IONPs was found to be about 50 emu/g, although this value decreased to 33.36 emu/g after modification with BSA NPs. The results revealed that encapsulation of IONPs with BSA NPs could result in reduction in magnetization.

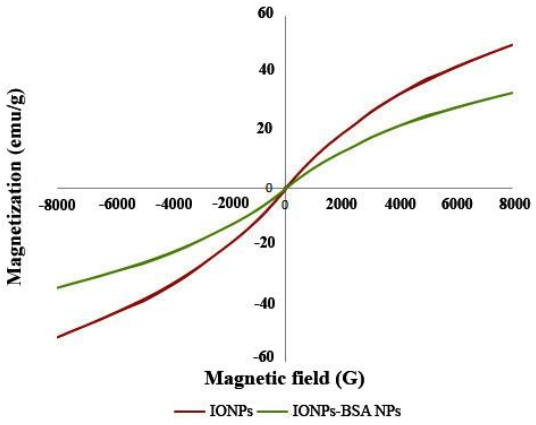

Fig 6. Magnetization curves of IONPs and IONPs-BSA nanoparticles

Decrease of magnetization per unit mass in the IONPs-BSA NPs may be due to the decreased mass of IONPs in comparison with the pure IONPs and also the presence of protein crona forming around the IONPs.

Stability studies

Storage stability of IONPs-BSA NPs during 6 months in aqueous solution (distilled water) without any preservative agent was evaluated in terms of physicochemical properties. Based on the results (Fig 7), size and zeta-potential of the system remained nearly unchanged during 4 months of storage at 4 ˚C, but PDI of IONPs-BSA NPs increased from 0.222 to 0.4 after 4 months, which could be due to the IONPs release from BSA NPs, particle adherence or degradation of the NPs under these conditions.

Stability results demonstrated that more than 90% and 60% of the particles retained their characteristics over four and six months, respectively, when stored at 4˚C under refrigerator conditions. However, they were still in an acceptable size range and zeta-potential fto be used as a MRI contrast agent.

Hemolysis assay

The hemolytic potential of all intravenously administered nanoprobs must be evaluated and *in vitro* evaluation of their biocompatibility with blood components is a necessary part of early preclinical development tests [33].

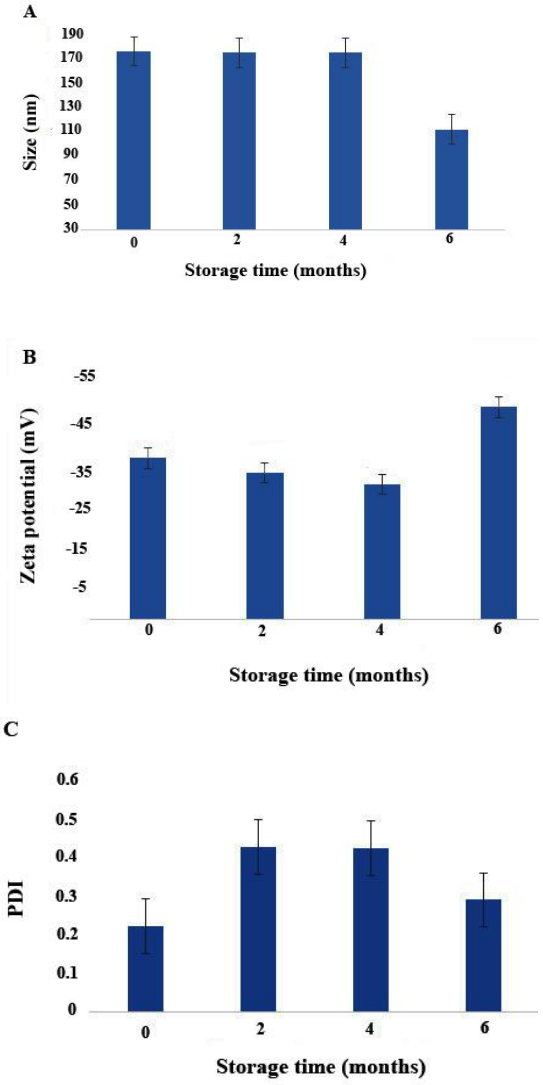

Fig 7. Long-term physicochemical stability of IONPs-BSA nanoparticles. (A) Particle diameter (nm), (B) Zeta potential (mV), and (C) Polydispersity index (PDI) recorded over a period of 6 months storage at 4 ºC (n = 3, mean ± SD)

The hemocompatibility of the formed IONPs-BSA NPs was evaluated by *in vitro* hemolysis assay. Figure 8 shows that both IONPs and the IONPs-BSA NPs exhibit good hemocompatibility, similar to the PBS (negative control). In contrast, the human red blood cells (HRBCs) exposed to deionized water (positive control) display apparent hemolysis behavior.

The hemolysis percentage of the NPs was quantified based on the absorbance of the supernatant at 541 nm. Hemolysis percentages

of both NPs are less than 10 % in the studied concentration range (0, 50, 100, 200, 400 µg/ml), suggesting their good hemocompatibility. However, studies revealed that IONPS-BSA NPs had better hemocompatibility than the IONPs. Therefore, BSA protects RBCs from hemolysis by ONPs.

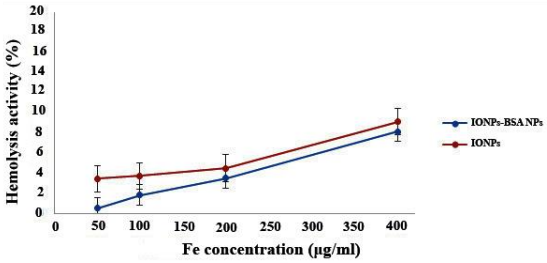

Fig 8. Hemolytical activity of the IONPs and IONPs-BSA NPs at different iron concentrations (0, 50, 100, 200, and 400 µg/ml). PBS and DI water were used as negative and positive control, respectively

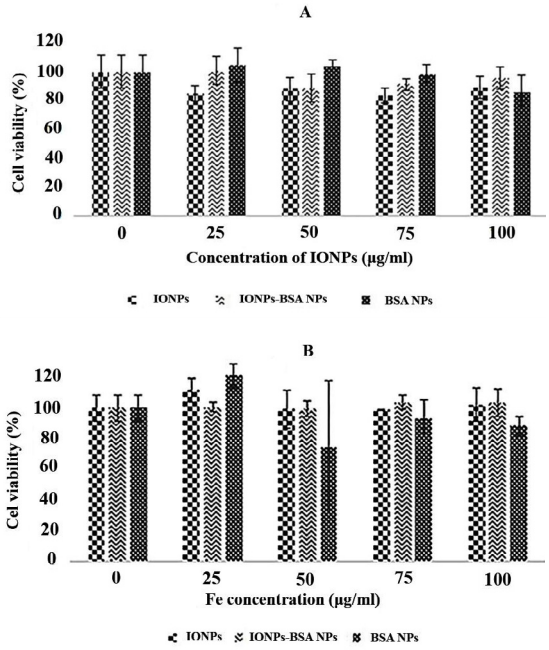

Fig 9. In vitro cytotoxicity test of IONPs, IONPs-BSA NPs, and BSA NPs. The viability of the MCF-7 cells determined by MTT assay after incubation with various concentrations of iron for 24 h (A) and 48 h (B). The obtained relative values were normalized to the values from corresponding untreated cells and are shown as percentage survival (n=3, mean ± SD)

In vitro cytotoxicity

Fig 9 demonstrates the cytotoxicity of IONPs, BSA NPs, and IONPs-BSA NPs in MCF-7 cells. Viability of over 80% was observed for MCF-7 cells after incubation with IONPs, BSA NPs, or IONPs-BSA NPs for 24 h and 48 h by increasing the iron concentration from 25 to 100 µg/ml. At the highest tested dose (100 µg iron/ml), minor effects on cell viability was observed after 24 and 48 h of incubation, indicating that the IONPs-BSA NPs, IONPs and BSA NPs have no obvious cytotoxicity. However, IONPs-BSA NPs showed lower toxicity than IONPs and BSA NPs, at relatively high iron concentrations of the 100 µg/ml for 24 or 48 h. According to the results, IONPs-BSA NPs showed excellent biocompatibility.

Hence, it can be concluded that the cytotoxicity of IONPs is reduced due to the biocompatible nature of BSA. The results were also in agreement with other reports showing non-toxicity of blank albumin NPs on different cells [20].

DISCUSSION

The successful application of IONPs in biomedical field is related specially to their magnetic properties, their dispersion and degree of aggregation [17]. Unmodified IONPs are rapidly cleared from the blood circulation. Surface modification with albumin might partially protect IONPs from being opsonized, reduce their clearance from blood [9, 34] and help to improve the local concentration of IONPs at the target sites of tumor and promoting the EPR effect *in vivo*, which plays a fundamental role in realizing passive targeting effect of IONPs.

According to previous reports, NPs smaller than 200 nm is preferentially accumulated in tumor tissues due to the EPR effect and may exhibit long blood circulation effects by avoiding recognition by the RES [19]. Extravasation and accumulation of larger particles in the tumor interstitium is slower compared to smaller ones, but they are retained for a longer time within the tumor tissue than smaller molecules, which are rapidly clear by diffusion [34]. The pore cutoff size of porous blood vessels in majority of tumors is known to be 380–780 nm [35], and the maximum size of NPs allowing penetration through cell membranes is known to be 500 nm [36]. The optimal nanocarrier size, often quoted to be in the size range of 50–200 nm [37]. Although the average hydrodynamic particle size of the prepared IONPs-BSA NPs is about 177 nm, which is larger than commercialized contrast agents, Feridex and Endorem (80-150 nm), Resovist (62 nm), Combidex and Sinerem (20-40 nm) [11], but it still can extravasate into the

tumor interstitium and become accumulated in the tumor tissue.

Proper aqueous solubility is one of the most important physicochemical factors that has been reported to play a major role in enhancing the NPs bioavailability. Importantly, serum albumin plays the major role as an "*in vivo* solubilizing agent" by enabling the water dispersibility of IONPs in hydrophilic media, (i.e. plasma). IONPs-BSA NPs were readily soluble in PBS (pH 7.4) or water, whereas free IONPs are insoluble [19].

In the present study, IONPs-BSA NPs were prepared by desolvation method which enabled the entrapment of hydrophobic IONPs into the biodegradable and biocompatible BSA; then the process was optimized by using CCD-RSM followed by analysis of the results by DX-7. The incorporation of the IONPs into the BSA matrix was confirmed by FTIR spectroscopy analysis. The entrapment of the IONPs was verified by VSM analysis of IONPs-BSA NPs. VSM analysis demonstrated that prepared IONPs-BSA NPs under optimum conditions had superparamagnetic properties. The loading efficiency obtained to be 7.71±0.23%. Findings revealed that desolvation method can be employed effectively for the production of MRI contrast agent, due to its simplicity, well defined conditions and reproducibility.

The *in vitro* toxicological tests were performed in the present study on MCF-7 cell viability and hemocompatibility. The results indicated that optimized IONPs-BSA NPs were non-cytotoxic and hemocompatible at the concentration up to 400 µg/ml. However, biocompatibility studies require not only hemolytic activity and *in vitro* cytotoxicity, but also cell uptake investigations and cytokine response should also be included, because of the discrepancies between *in vitro* tests under static conditions and the dynamic conditions in the blood stream, limiting the translating of 2D-cell culture data to the *in vivo* situation [38]. Furthermore, cell culture systems do not sufficiently represent the complexity of interactions between nanomaterials and the different components relevant to systemic administration such as blood vessel walls, blood cells, and serum proteins [39].

The synthesized IONPs-BSA NPs exhibited excellent stability in deionized water without precipitation, even for up to 4 months storage at 4 °C, that can be due to their remarkably negative zeta potential, which prevents the IONPs-BSA NPs from agglomeration in the colloid state. These results are concomitance with the long term storage results obtained for CAN maghemite-containing rHSA NPs [16]. Rosenberger et al. showed that the optimal storage temperature for CAN maghemite-containing rHSA NPs was 2-8 °C, consequently cold conditions were not necessary, and no relevant changes were observed after 12 weeks of storage, in terms of alteration in size and polydispersity.

As shown in previous studies, positively charged NPs show a faster uptake by cells and a higher opsonization rate than highly anionic NPs, resulting in a higher uptake of the NPs by the RES because of their interaction with human blood proteins such as albumin and IgG16. But negatively charged IONPs-BSA NPs are protected from opsonization by negatively charged blood proteins, thereby prolonging the circulating half-lives which translated to improved accumulation in tumors [40].

The particles developed in the present study can also be considered as a promising active targeted imaging tool, because of their feasibility of shell functionalization by introduction of targeting ligands. MR imaging plays a major role in diagnosis of tumors, because MRI allows an anatomical analysis of the scanned areas [41]. These features may allow further development of the presented NPs for tumor imaging. The functional groups on the surface of BSA particle allow the attachment of potential ligands, which may enable an active targeting of the NPs specifically targeting the tumor tissue [21, 40, 42, 26, 29, 43-45].

CONCLUSION

In this study, an MRI contrast agent based on IONPs-BSA NPs was prepared by optimized desolvation method. BSA NPs, as a biodegradable nontoxic carrier, was loaded with a high amount of IONPs under optimum conditions (2.28 mg iron weight, 9.21 pH). Particles produced under optimum conditions, had the average size of 177±12 nm, zeta potential of -36.42±2.3 mV and PDI of 0.2±0.07. The produced NPs were at acceptable ranges of physicochemical properties after long-term storage. The IONPs-BSA NPs developed in the present study are promising to be further investigated and functionalized with a ligand to obtain a targetable MRI contrast agent for early cancer diagnosis. The particle size, morphology and stability analysis indicated that

the IONPs-BSA NPs were quite stable, spherical in shape and sizes within the optimal range for imaging applications. The MTT results support the nontoxic nature of the IONPs-BSA NPs. In general, these results suggest that the IONPs-BSA NPs may be useful as vehicles for IONP contrast agent. However, it should be noted that this study utilizes BSA as a proof-of-concept investigation. In future, HSA would be considered instead of BSA to avoid probable immunologic consequences for *in vivo* trials. Thus, our study proposes that the imaging potential of IONPs could be better utilized by loading them under an optimum condition, in a protein-based carrier for future clinical applications.

REFERENCES

1.Siegel RL, Miller KD, Fedewa SA, Ahnen DJ, Meester RGS, Barzi A, Jemal A. Colorectal Cancer Statistics, 2017. CA Cancer J Clin. 2017; 67(3): 177-193.

2.Sanjai C, Kothan S, Gonil P, Saesoo S, Sajomsang W. Chitosan-triphosphate nanoparticles for encapsulation of super-paramagnetic iron oxide as an MRI contrast agent. Carbohydr Polym. 2014; 104: 231–237.

3.Sun C, Lee JJSH, Zhang M. Magnetic nanoparticles in MR imaging and drug delivery. Adv Drug Del Rev. 2008; 60: 1252–1265.

4.Albanese C, Rodriguez OC, VanMeter J, Fricke ST, Rood BR, Lee Y, Wang SS, Madhavan S, Gusev Y, 3rd Petricoin EF, Wang Y. Preclinical magnetic resonance imaging and systems biology in cancer research: current applications and challenges. Am J Pathol. 2013; 182: 312–318.

5.Maboudi SA, Shojaosadati SA, Arpanaei A. Synthesis and characterization of multilayered nanobiohybrid magnetic particles for biomedical applications. Mater Des. 2017; 115: 317-324.

6.Li J, He Y, Sun W, Luo Y, Cai H, Pan Y, Shen M, Xia J, Shi X. Hyaluronic acid-modified hydrothermally synthesized iron oxide. Biomaterials. 2014; 35: 3666–3677.

7.Rosenberger I, Strauss A, Dobiasch S. Targeted diagnostic magnetic nanoparticles for medical imaging of pancreatic cancer J. Control Rel. 2015; 214: 76–84.

8.Hong GB, Zhou J, Yuan R. Folate-targeted polymeric micelles loaded with ultrasmall superparamagnetic iron oxide. combined small size and high MRI sensitivity. Int J Nanomedicine. 2012; 7: 2863-2872.

9. Xie J, Zhang Y, Yan C, Song L, Wen S, Zang F, Chen G, Ding Q, Yan C, Gu N. High-performance PEGylated Mn-Zn ferrite nanocrystals as a passive-targeted agent for magnetically induced cancer theranostics. Biomaterials (2014); 35: 9126–9136.

10. Frangioni JV. New technologies for human cancer imaging. J Clin Oncol. 2008; 26: 4012–4021.

11. Jun YW, Lee JH, Cheon J. Chemical design of nanoparticle probes for high-performance magnetic resonance imaging. Angew Chemie - Int Ed. 2008; 47: 5122–5135.

12.Kandasamy G, Maity D. Recent advances in superparamagnetic iron oxide nanoparticles (SPIONs) for in vitro and in vivo cancer nanotheranostics. Int J Pharm. 2015; 496: 191–218.

13. Pysz MA, Gambhir SS, Willmann JK. Molecular imaging: current status and emerging strategies. Clin Radiol. 2010; 65: 500–516.

14. Weissleder R. Scaling Down Imaging: Molecular Mapping of Cancer in Mice. Nat Rev Cancer. 2002; 2: 11–18.

15. Weissleder R, Mahmood U. Molecular Imaging, Radiology. 2001; 219: 316–333.

16. Rosenberger I, Schmithals C, Vandooren J. Physico-chemical and toxicological characterization of iron-containing albumin nanoparticles as platforms for medical imaging. J Control Rel. 2014; 194: 130–137.

17.Lima-Tenorio MK, Gomez Pineda EA, Ahmad NM, Fessi H, Elaissari A. Magnetic nanoparticles: In vivo cancer diagnosis and therapy. Int J Pharm. 2015; 493: 313–327.

18.Ghosh P, Patwari J, Dasgupta S. Complexation with Human Serum Albumin Facilitates Sustained Release of Morin from Polylactic-Co-Glycolic Acid Nanoparticles. J Phys Chem B. 2017; 121: 1758–1770.

19.Singh P, Singh H, Castro-Aceituno V, Ahn S, Kim YJ, Yang DC. Bovine serum albumin as a nanocarrier for the efficient delivery of ginsenoside compound K: preparation, physicochemical characterizations and in vitro biological studies. RSC Adv. 2017; 7: 15397–15407.

20.Kouchakzadeh H, Shojaosadati SA. The prominent role of protein-based delivery systems on the development of cancer treatment. Curr Pharm Des. 2016; 22: 3455-3465.

21. Li H, Yan K, Shang Y, Shrestha L, Liao R, Liu F, Li P, Xu H, Xu Z, Chu PK. Folate-bovine serum albumin functionalized polymeric micelles loaded with superparamagnetic iron oxide nanoparticles for tumor targeting and magnetic resonance imaging. Acta Biomater. 2015; 15: 117-126.

22.Mariam J, Sivakami S, Dongre PM. Albumin corona on nanoparticles–a strategic approach in drug delivery. Drug Deliv. 2016; 23: 2668–2676.

23. Kouchakzadeh H, Soudi T, Heshmati Aghda N, Shojaosadati SA. Ligand-modified Biopolymeric Nanoparticles as Efficient Tools for Targeted Cancer Therapy. Curr Pharm Des. 2016; 23: 5336-5348.

24.Langer K, Anhorn MG, Steinhauser I, Dreis S, Celebi D, Schrickel N, Faust S, Vogel V. Human serum albumin (HSA) nanoparticles: Reproducibility of preparation process and kinetics of enzymatic degradation. Int J Pharm. 2008; 347: 109–117.

25.Kouchakzadeh H, Safavi MS, Shojaosadati SA. Efficient delivery of therapeutic agents by using targeted albumin nanoparticles. Adv Protein Chem Struct Biol. 2015; 98: 121–143.

26.Kouchakzadeh H, Shojaosadati SA, Tahmasebi F, Shokri F. Optimization of an anti-HER2 monoclonal antibody targeted delivery system using PEGylated human serum albumin nanoparticles. Int J Pharm. 2013; 447: 62–69.

27.Kouchakzadeh H, Shojaosadati SA, Maghsoudi A, Vasheghani Farahani E. Optimization of PEGylation conditions for BSA nanoparticles using response surface methodology. AAPS PharmSciTech. 2010; 11: 1206–1211.

28. Jun JY, Nguyen HH, Paik SYR, Chun HS, Kang BC, Ko S. Preparation of size-controlled bovine serum albumin (BSA) nanoparticles by a modified desolvation method, Food Chem. 2011; 127: 1892–1898.

29.Kouchakzadeh H, Shojaosadati SA, Shokri F. Efficient loading and entrapment of tamoxifen in human serum

albumin based nanoparticulate delivery system by a modified desolvation technique. Chem Eng Res Des. 2014; 92: 1681–1692.
30. Ishay RB, Israel LL, Eitan EL, Partouche DM, Lellouche JP. Maghemite-human serum albumin hybrid nanoparticles: towards a theranostic system with high MRI r 2 * relaxivity, J Mater Chem B. 2016; 4: 3801–3814.
31.Deljoo Kojabad Z, Shojaosadati SA. Chemical synthesis of polypyrrole nanostructures: Optimization and applications for neural microelectrodes. Mater Des. 2016; 96: 378-384.
32.Dobrovolskaia MA, Clogston JD, Neun BW, Hall JB, Patri AK, McNeil SE. Method for Analysis of Nanoparticle Heolytic Properties In Vitro. Nano Lett. 2008; 8: 2180–2187.
33.Yamashita F, Hashida M. Pharmacokinetic considerations for targeted drug delivery. Adv Drug Deliv Rev. 2013; 65: 139–147.
34.Pirollo KF, Chang EH, Does a targeting ligand influence nanoparticle tumor localization or uptake?. Trends Biotechnol. 2008; 26: 552–558.
35.Hobbs SK, Monsky WL, Yuan F, Roberts WG, Griffith L, Torchilin VP, Jain RK. Regulation of transport pathways in tumor vessels: Role of tumor type and microenvironment. Proc Natl Acad Sci USA. 1998; 95: 4607–4612.
36. Baea YH, Park K. Targeted drug delivery to tumors: myths, reality and possibility. J. Control Release (2011); 153: 198–205.
37. Nel A, Ruoslahti E, Meng H. New Insights into 'permeability' as in the Enhanced Permeability and Retention Effect of Cancer Nanotherapeutics. ACS Nano. 2017; 11: 9567–9569.
38.Schleich N, Sibret P, Danhier P. Dual anticancer drug/superparamagnetic iron oxide-loaded PLGA-based nanoparticles for cancer therapy and magnetic resonance imaging. Int J Pharm. 2013; 447: 94–101.
39.Schlenk F, Werner S, Rabel M, Jacobs F, Bergemann C, Clement JH, Fischer D. Comprehensive analysis of the in vitro and ex ovo hemocompatibility of surface engineered iron oxide nanoparticles for biomedical applications. Arch Toxicol. 2017; 91: 3271–3286.
40.Blanco E, Shen H, Ferrari M. Principles of nanoparticle design for overcoming biological barriers to drug delivery. Nat Biotechnol. 2015; 33: 941–951.
41.Muthiah M, Park IK, Cho CS. Surface modification of iron oxide nanoparticles by biocompatible polymers for tissue imaging and targeting. Biotechnol Adv. 2013; 31: 1224–1236.
42.Ahmad T, Bae H, Iqbal Y, Rhee I, Hong S. Chitosan-coated nickel-ferrite nanoparticles as contrast agents in magnetic resonance imaging. J Magn Magn Mater. 2015; 381: 151–157.
43.Li ZY, Qin XY, Guo LY, Wang H, Liu XX, Zheng ZZ, Guan HT, Song L, Zou YH, Fan TY. Poly (acrylic acid) microspheres loaded with superparamagnetic iron oxide nanoparticles for transcatheter arterial embolization and MRI detectability: In vitro and in vivo evaluation. Int J Pharm. 2017; 527 (1-2); 31-41.
44.Song X, Luo X, Zhang Q, Zhu A, Ji L, Yan C. Preparation and characterization of biofunctionalized chitosan/Fe3O4 magnetic nanoparticles for application in liver magnetic resonance imaging. J Magn Magn Mater. 2015; 388: 116–122.
45.Wang J, Zhang B, Wang L, Wang M, Gao F. One-pot synthesis of water-soluble superparamagnetic iron oxide nanoparticles and their MRI contrast effects in the mouse brains. Mater Sci Eng C. 2015; 48: 416–423.